Nanomedicine

ISSN: (Print) (Online) Journal homepage: www.tandfonline.com/journals/innm20

Detection of Tn-antigen in breast and prostate cancer models by VVL-labeled red dye-doped nanoparticles

Alejandra Verhassel, Martha Kimani, Kamlesh Gidwani, Jouko Sandholm, Kornelia Gawlitza, Knut Rurack & Pirkko Härkönen

To cite this article: Alejandra Verhassel, Martha Kimani, Kamlesh Gidwani, Jouko Sandholm, Kornelia Gawlitza, Knut Rurack & Pirkko Härkönen (09 Oct 2024): Detection of Tn-antigen in breast and prostate cancer models by VVL-labeled red dye-doped nanoparticles, Nanomedicine, DOI: 10.1080/17435889.2024.2405454

To link to this article: https://doi.org/10.1080/17435889.2024.2405454

NANOMEDICINE
https://doi.org/10.1080/17435889.2024.2405454

Taylor & Francis
Taylor & Francis Group

RESEARCH ARTICLE

OPEN ACCESS Check for updates

Detection of Tn-antigen in breast and prostate cancer models by VVL-labeled red dye-doped nanoparticles

Alejandra Verhassel[‡,a,b], Martha Kimani[‡,c], Kamlesh Gidwani[b,d], Jouko Sandholm[e], Kornelia Gawlitza[*,c], Knut Rurack[c] and Pirkko Härkönen[**,a,b]

[a]Institute of Biomedicine, University of Turku, Turku, 20520, Finland; [b]Western Cancer Centre FICAN West, Turku, 20521, Finland; [c]Chemical and Optical Sensing Division, Bundesanstalt für Materialforschung und -prüfung (BAM), Berlin, 12489, Germany; [d]Department of Biochemistry, University of Turku, Turku, 20520, Finland; [e]Turku Bioscience Centre, University of Turku and Åbo Akademi University, Turku, 20520, Finland

ABSTRACT

Aim: Fluorescence detection of breast and prostate cancer cells expressing Tn-antigen, a tumor marker, with *Vicia villosa* lectin (VVL)-labeled nanoparticles.

Materials & methods: Breast and prostate cancer cells engineered to express high levels of Tn-antigen and non-engineered controls were incubated with VVL-labeled or unlabeled red dye-doped silica-coated polystyrene nanoparticles. The binding to cells was studied with flow cytometry, confocal microscopy, and electron microscopy.

Results: Flow cytometry showed that the binding of VVL-labeled nanoparticles was significantly higher to Tn-antigen-expressing cancer cells than controls. Confocal microscopy demonstrated that particles bound to the cell surface. According to the correlative light and electron microscopy the particles bound mostly as aggregates.

Conclusion: VVL-labeled nanoparticles could provide a new tool for the detection of Tn-antigen-expressing breast and prostate cancer cells.

ARTICLE HISTORY
Received 10 July 2024
Accepted 13 September 2024

KEYWORDS
breast cancer cells; fluorescence detection; lectin labeling; prostate cancer cells; silica-coated polystyrene nanoparticles; Tn-antigen; VVL

GRAPHICAL ABSTRACT

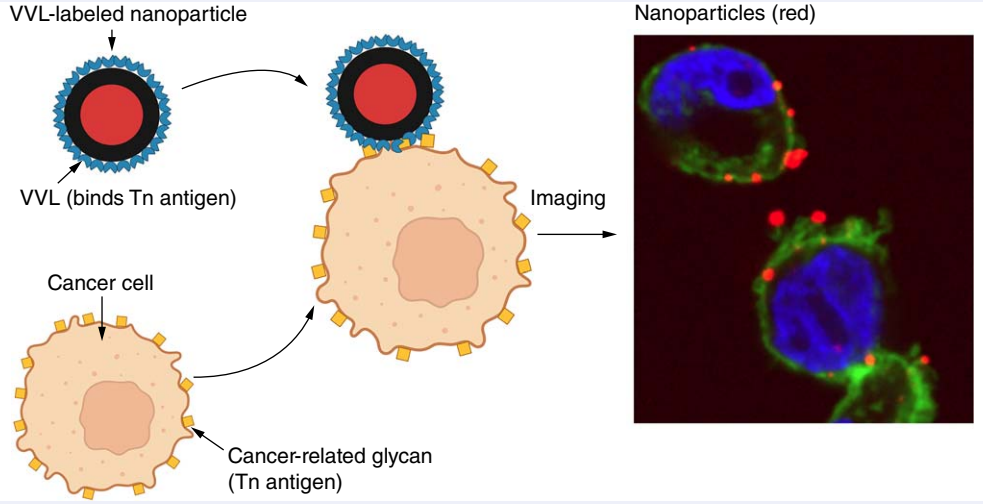

1. Introduction

Protein glycosylation is a post-translational modification, in which a carbohydrate chain (glycan) is attached to a protein, forming a glycoprotein [1,2]. Glycans influence cell membrane properties, support cell signaling and attachment, and influence protein folding and stability [2,3]. The two most common and important forms of

CONTACT Kornelia Gawlitza kornelia.gawlitza@bam.de; Pirkko Härkönen harkonen@utu.fi

‡Equal contribution

Supplemental data for this article can be accessed at https://doi.org/10.1080/17435889.2024.2405454

human protein glycosylation are *N*-glycosylation (glycan chain bound to an asparagine) and *O*-glycosylation (glycan chain bound to serine (Ser), threonine (Thr), or tyrosine (Tyr)) [1,4]. *O*-glycosylation can be further subdivided into different types, depending on which carbohydrate is linked to the protein (e.g., linkage of *N*-acetylgalactosamine (GalNAc) or N-acetylglucosamine (GlcNAc) and which enzymes are responsible for linking the first carbohydrate to the protein (e.g., GALNT1 or OGT, respectively) [3].

Changes in the structure of cell-surface glycans are related to various diseases [5], including malignancies [6–8]. A common alteration in cancer cells is the presence of truncated *O*-GalNAc glycans, such as the Tn-antigen and its sialylated form Sialyl-Tn-antigen (STn-antigen) [4,9]. The Tn-antigen, consisting of a GalNAc linked to a Ser or Thr residue, is present in >80% of breast, 72–81% of colon and 4–26% of prostate cancers [10–13]. In addition, Tn-antigen is expressed in many other cancer types [4]. Therefore, the Tn-antigen could act as a marker for various cancers, particularly at their early stages, and could thus be applied in early cancer diagnosis [14,15].

Current methods of detecting Tn-antigen are based on the use of lectins (such as VVL) and antibodies [15–18]. Silva and coworkers coupled VVL to gold electrodes and utilized electrical impedance spectroscopy to monitor the binding of Tn-antigen-containing glycoproteins [19]. Pinto et al. employed antibodies in an in-situ proximity ligation assay to identify Tn-antigen structures in mucins present on stomach, breast and ovarian adenocarcinomas [20]. Even though the antibodies are widely used and new specific antibodies have recently been developed [18], they are costly and easily inactivated [15]. Lectins have disadvantages such as limited sensitivity and affinity (the dissociation constant (KD) for monovalent carbohydrates is in the mM range) [21]. Therefore, new alternative diagnostic technologies would be useful [22].

Stable cell labeling agents containing fluorescent markers have been developed to stain Tn-antigen-expressing cells, and the presence or absence of Tn-antigen can thereafter be directly determined by quick read-out assays. Gidwani and coworkers studied the binding of human lectin- and anti-STn antibody-conjugated europium chelate-dyed polystyrene (PS) nanoparticles to immobilized serum cancer antigen 125 (CA125; a biomarker for epithelial ovarian cancer) in patient serum in a glycovariant assay. The binding affinities of the nanoparticle conjugates were compared with that of individual lectins fluorescently labeled with europium chelates. They showed that the particle-conjugated lectins and antibodies displayed stronger affinities to the target biomarkers compared with their unconjugated counterparts. Therefore, immobilization of lectins and antibodies at high density on the particle surface enhanced the binding strength to the targets via the avidity effect [23,24].

Nanoparticles to be used as fluorescent cell labeling agents for glycoproteins expressed on cell surfaces should be tailored in size and surface chemistry to show high binding efficiency and a sufficiently long residence time [25,26]. While quantum dots (QDs) decorated with receptors have been widely used as fluorescent probes for biological applications, toxic and costly materials are typically required for their synthesis, in addition to the need to optimize their synthesis to influence their fluorescence emission properties. Polymer particles are a suitable alternative, since their synthesis is cost-effective, and they can be doped with a wide range of organic dyes to achieve desired fluorescence properties. Dye-doped polymer particles such as polymethylmethacrylate (PMMA) and PS beads have been developed for a wide range of applications [27–31].

In this study, we developed and validated new red dye-doped silica-coated PS nanoparticles labeled with VVL for the detection of Tn-antigen on breast and prostate cancer cell lines. By combining a high number of lectins on a small surface, we expect to overcome one of the main limitations occurring when only lectins are used for detecting glycans. The low binding capacity of the individual lectin is expected to be improved by increasing the number of interactions between lectins and glycans and the opportunities to bind to the cancer-related glycan [32]. The red-fluorescent dye makes them suitable for *in vitro* applications and possibly, *in vivo* work in the future. The particles were additionally grafted with polyethylene glycol (PEG) moieties to passivate the particle surface and reduce non-specific binding [31–35]. The use of lectin-labeled particles has been used for microarray assay. In this study, we aim to use novel particles, doped with a red dye, for detection techniques that could -in a later step- lead to other clinical applications.

As cell models, we used two different breast cancer cell lines (MDA MB 231 and MCF7) and a prostate cancer cell line (PC-3), all of which had been glycoengineered to express Tn-antigen at a high level by the SimpleCell technique [36]. This technique uses zinc finger nuclease-based gene editing to knockout (KO) COSMC, a private chaperone of C1GalT1, a protein responsible for elongating *O*-glycosylation [37]. Inactivation of the *COSMC* gene causes a limitation in the GalNAc-type O-glycosylation capacity in cells. By this, GalNAc glycans are simplified to Tn- and STn-antigens.

Particle binding was studied with flow cytometry and confocal microscopy for MDA MB 231, MCF7 and PC-3. The binding pattern of the PEGylated particles was visualized for MDA MB 231 SC and WT cells and the

MDA MB 231 cells stained with the PEGylated particles were further imaged with correlative light and electron microscopy (CLEM).

2. Materials & methods

2.1. Materials

A description of all materials is reported in supporting information (SI) section 1.

2.2. Synthesis of fluorescent dye & particles

2.2.1. Synthesis of doping dye I, 3,5-bis(4-methoxyl styryl)-8-pentafluorophenyl-4,4-difluoro-4-bora-3a,4a-diaza-s-indacene

Dye **I** was synthesized as previously reported (^{1}H NMR characterization presented in SI section 2a, Supplementary Figure S1) [38].

The synthesis of positively charged PS particles is described in SI, section 2b.

Dye doping and silica coating of PS is described in SI, section 2c.

2.2.2. Coating of dye-doped silica-coated particles with a secondary silica shell

500 mg of the silica-shelled particles were suspended in 8.9 ml Milli-Q water and 33.2 ml absolute ethanol with 10 min sonication. 2.9 ml of 32% ammonia was then added and 3.5 ml TEOS (15.7 mmol) was introduced into the solution at a rate of 0.01 ml min^{-1} using a syringe pump with stirring at 300 rpm. After dosing was complete, the reaction was allowed to continue for 35 min. The particles were washed three-times with 96% ethanol, with centrifugation at 12,700 $\times g$ for 10 min, with 5 min sonication between washes. The resulting particles (**SiO_2@PS**, 1600 mg) were dried overnight under a vacuum.

2.2.3. APTES & PEG modification of SiO_2@PS

50 mg of **SiO_2@PS** were weighed out separately in two 2 ml Eppendorf tubes and dispersed in 1.2 ml absolute ethanol with 5 min sonication, then 0.6 ml water:37% HCl 9:1 was added and the mixtures were sonicated for 10 min. The particles were centrifuged at 10,000 $\times g$ for 5 min, then washed twice with 1.2 ml absolute ethanol with 5 min sonication between washes and centrifugation at 10,000 $\times g$ for 5 min. The particles were resuspended in 1 ml absolute ethanol with 5 min sonication. In one tube, 50 μl APTES (47.3 mg, 0.2 mmol) was added. To the other tube, 25 μl APTES (23.7 mg, 0.1 mmol) and 25 μl 3-[methoxy(polyethyleneoxy)propyl]trimethoxysilane (26.9 mg, average 0.1 mmol) were added. Both suspensions were mixed for 23 h in a thermomixer at 750 rpm and 40°C. Afterward, the particles were purified by washing three-times with 1 ml absolute ethanol, with centrifugation at 10,000 $\times g$ for 5 min after each wash. The APTES-modified particles (**A@SiO_2@PS**) and APTES/PEG-modified particles (**AP@SiO_2@PS**) were dried in a vacuum oven overnight.

2.2.4. COOH functionalization of A@SiO_2@PS & AP@SiO_2@PS particles

30 mg each of **A@SiO_2@PS** and **AP@SiO_2@PS** particles were suspended in 1 ml absolute ethanol with 10 min sonication. 80 mg of succinic anhydride (0.8 mmol) was dissolved in 400 μl Dimethylformamide. 100 μl of the solution was added to each vial. The particle suspensions were mixed for 18 h in a thermomixer at 1000 rpm and 40°C. Afterward, the particles were purified by washing three-times with 1 ml absolute ethanol, with centrifugation at 10,000 $\times g$ for 3 min after each wash. The resulting particles (**CA@SiO_2@PS** (shortened to **CA**) and **CAP@SiO_2@PS** (shortened to **CAP**)) were dried in a vacuum oven overnight.

Conjugation of VVL to CA@SiO_2@PS and CAP@SiO_2@PS is described in SI, section 2d. The obtained particles were **VVL-CA@SiO_2@PS** (shortened to **VVL-CA**, for particles with amino groups on the surface) and **VVL-CAP@SiO_2@PS** (shortened to **VVL-CAP**, for particles with amino and PEG groups on the surface).

2.3. In vitro cell experiments

2.3.1. Materials

SC cell lines were engineered at the Center of Glycomics (Prof. Henrik Clausen, University of Copenhagen, Denmark) as described in SI, Section 3 and cultured in-house [36]. HEK293T cells were kindly provided by Cecilia Sahlgren's laboratory (Åbo Akademi University). 10 cm cell culture plates and 24-well plates were obtained from Corning. 96 well plates were obtained from Greiner Bio-One. Gridded coverslips used for CLEM were kindly provided by Dr. Markus Peurla (Laboratory of Electron Microscopy, Institute of Biomedicine, University of Turku).

2.3.2. Cell lines & in vitro cultures

Human breast cancer cell lines MDA MB 231 WT, MDA MB 231 SC, human prostate cancer cell line PC-3 WT, PC-3 SC and HEK 293T cells were cultured in DMEM medium, supplemented with 10% inactivated fetal bovine serum, 1% l-glutamine and 1% penicillin-streptomycin for human breast cancer cell line MCF7 WT and MCF7 SC 10 μg ml^{-1} insulin (human recombinant, zinc solution) was added. Cells were kept in an incubator at 37°C and 5% CO_2. Cells were authenticated by the

IdentiCell STR profiling service (Department of Molecular Medicine, Aarhus University Hospital, Denmark). Regular mycoplasma tests were performed with the Lonza LT07-118 kit. Unconjugated and biotinylated VVL was obtained from Vector Laboratories and Alexa Fluor 488-conjugated streptavidin was obtained from Thermo Fisher Scientific.

The engineered cell lines are referred to as SimpleCells (SC) [34]. The corresponding non-engineered ("wild-type", WT) cancer cells were used as controls. As an extra control, we used HEK293T cells as a non-cancerous cell line. WT, SC and HEK293T cells were incubated with PEGylated/nonPEGylated VVL-labeled nanoparticles (further referred to as **VVL-CAP/VVL-CA**) as well as the corresponding PEGylated/nonPEGylated unlabeled control nanoparticles (further referred to as **CAP/CA**).

2.3.3. Flow cytometry

A total of 1×10^5 cells were used per well in a 96-well plate. Cells were incubated with 50 μl of biotinylated VVL in PBS (0.01 mg ml^{-1}) or **VVL-CA**, **VVL-CAP**, **CA** and **CAP** (0.05 mg ml^{-1}) for 30 min in the dark and on ice. Cells that were incubated with biotinylated VVL were further incubated with 50 μl of AlexaFluor 488-conjugated streptavidin in PBS (dilution 1:1000) for 30 min in the dark and on ice. Fluorescently tagged cells (with biotinylated VVL/streptavidin Alexa Fluor 488 or **VVL-CA**, **VVL-CAP**, **CA** and **CAP**) were analyzed with flow cytometry.

2.3.4. Staining of fixed cells with particles

A total of 5×10^4 cells were plated on a 24-well plate on sterile coverslips. The plates were put overnight in an incubator at 37°C and 5% CO_2. The next day cells were fixed with 4% paraformaldehyde (200 μl per well) for 15 min at room temperature. On the day of staining, PBS was removed and the cells were incubated in the dark at RT with biotinylated VVL in 200 μl PBS at a final concentration of 10 μg ml^{-1} (200 μl per well; 1 μl of the stock solution of biotinylated VVL in 200 μl PBS). Next, cells were incubated with 200 μl of AlexaFluor 488-conjugated streptavidin in PBS (dilution 1:1000) for 30 minutes at RT and in the dark. Then, cells were incubated with 200 μl of Phalloidin in PBS (dilution 1:300; to stain F-actin) and 200 μl Hoechst 33342 dye in PBS (dilution 1: 1500; to stain nuclei) for 5 min. For staining with **VVL-CA**, **VVL-CAP**, **CA** and **CAP,** the particles were treated similarly, except that the cells were incubated with the particles at a concentration of 0.05 mg ml^{-1} before the fixation step. The incubation was done on ice and in the dark for 30 min. Coverslips were mounted on microscope slides and stored in the dark at 4°C until imaging. For imaging with the scanning electron microscope (SEM), samples were not mounted on coverslips after incubation with the nanoparticles but were fixed with 2% glutaraldehyde (EM grade) in 0.2 M HEPES for 120 min at RT. Before imaging with the SEM, samples were sputter-coated with platinum (thickness 6 nm).

2.3.5. Instrumentation & software

All instrumentation and software are presented in SI section 1.

3. Results

3.1. Synthesis & characterization of dye-doped particles for lectin conjugation

PS particles were chosen as core particles. Using a published protocol [39], cationic PS nanoparticles were synthesized by suspension polymerization in aqueous media. The resulting aqueous suspension of the PS particles was thereafter incubated with a THF solution of dye **I** for 30 min to allow the imbibing of the dye into the particles. The red-emitting fluorescent dye **I** (Figure 1A) containing a BODIPY core was used as a dopant [38]. In THF, absorption occurs at 669 nm, and emission is observed at 691 nm following excitation at 600 nm (Figure 1B). After dye-doping, silica coating was necessary to allow easy functionalization of the particle surface, and to protect the PS core from dye loss in subsequent functionalization steps carried out to facilitate lectin conjugation. The suspension of dye-doped PS particles was therefore diluted in water, and silica coating was performed in aqueous media using l-lysine as a catalyst. This first silica shell was too porous to adequately protect the doped PS core, therefore, a denser secondary silica shell was synthesized on the surface of the first silica shell following a modified Stöber method [40,41]. The absorption and fluorescence spectra of the dye-doped silica particles (**SiO_2@PS**) showed that the doping process was successful (Figure 1B). Compared with the dye in THF, the absorption and emission were red-shifted to 682 nm and 694 nm, respectively. Considering also the band maxima in toluene, the shifts can be entirely attributed to dispersive interactions (Supplementary Figure S2, SI section 4).

To conjugate VVL to **SiO_2@PS**, it was necessary to further functionalize the silica surface with appropriate anchoring groups like carboxylic acid groups. The particles were first reacted with APTES to introduce amino groups on the surface (**A@SiO_2@PS**), after which the particles were reacted with succinic anhydride to yield carboxylic acid groups (**CA@SiO_2@PS**, shortened to **CA**). To investigate the effect of PEGylation on the particle behavior, **SiO_2@PS** particles were also reacted with APTES and a PEGylated silane (3-[methoxy(polyethylene oxy)propyl]trimethoxysilane) simultaneously, to intro-

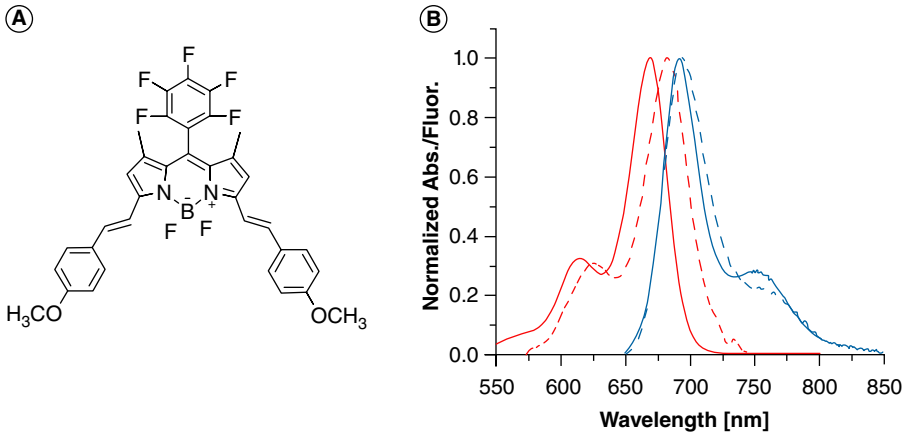

Figure 1. **(A)** Structure of fluorescent doping dye **I**. **(B)** Normalized absorption (solid red line) and fluorescence emission spectra (solid blue line) in THF (1 μM). Normalized absorption (dashed red line) and fluorescence emission spectra (dashed blue line) of 1 mg ml^{-1} dye-doped **SiO_2@PS** suspended in ethanol. Particle spectra were corrected for scattering effects. $\lambda_{ex} = 600$ nm.

duce amino and PEG groups on the surface, yielding **AP@SiO_2@PS**. These particles were also reacted with succinic anhydride to yield particles with PEG groups and carboxylic acid groups on the surface (**CAP@SiO_2@PS**, shortened to **CAP**) (Figure 2).

To determine the number of accessible amino groups on the surface of **A@SiO_2@PS** and **AP@SiO_2@PS**, as well as the conversion to carboxylic acid groups in **CA** and **CAP**, the ninhydrin test was performed (Supplementary Figure S3, SI section 5). **A@SiO_2@PS** and **AP@SiO_2@PS** contained 0.45 and 0.14 mmol g^{-1} of (accessible) amino groups, respectively. No amino groups were detected in **CA** and **CAP**, demonstrating the successful conversion of surface amino groups. Based on the specific surface area of **SiO_2@PS** determined from porosimetry (37.7 m^2 g^{-1}, Supplementary Figure S4, SI section 6), the density of amino groups grafted onto the surface of **A@SiO_2@PS** and **AP@SiO_2@PS** was calculated to be 7.2 groups nm^{-2} and 2.2 groups nm^{-2} respectively. Since the virtually quantitative conversion of the amino groups to carboxylic groups was accomplished based on the results of the ninhydrin test, carboxylic acid group densities on **CA** and **CAP** should be comparable, respectively (Supplementary Figure S3, SI).

The synthesized particles were further characterized by TEM, zeta potential and TGA measurements. From statistical analysis of TEM images, the PS nanoparticles have a diameter of 40 $\pm$ 8 nm (Figure 3A). The overall silica shell thickness of **SiO_2@PS** was determined to be 18 $\pm$ 2 nm resulting in a final particle size of 76 $\pm$ 11 nm (Figure 3B). As expected from zeta potential measurements (SI section 7), the PS particles displayed positive potential due to the protonated amino groups on the outer surface supplied by the AIBA initiator used during PS synthesis, while **SiO_2@PS** possessed a negative surface charge from the silanol groups on the outer surface. Modification with APTES led to the reintroduction of amino groups on the surface for **A@SiO_2@PS** and **AP@SiO_2@PS** and consequently, a net positive charge, which was reduced for **CA** and **CAP** after condensation of the amino groups with succinic anhydride (Figure 3C). The PEG chains introduced onto the particle surface possess a neutral charge and were not expected to influence the surface charge of the particles. TGA measurements indicated mass loss from the combustion of covalently attached organic groups on the particle surface with increasing temperature (Figure 3D). The mass loss increased from 0.9% to 1.8% for **A@SiO_2@PS** and **AP@SiO_2@PS**, respectively. Together with the decrease in accessible amino groups stated before (7.2 groups nm^{-2} and 2.2 groups nm^{-2}), one can conclude that **AP@SiO_2@PS** are indeed functionalized with a mixture of APTES groups and PEG chains.

CA and **CAP** were then conjugated to VVL using sulfo-NHS and EDC in phosphate buffer as previously reported [23,24]. The obtained particles were **VVL-CA@SiO_2@PS** (shortened to **VVL-CA**, for particles with amino groups on the surface) and **VVL-CAP@SiO_2@PS** (shortened to **VVL-CAP**, for particles with amino and PEG groups on the surface). The affinity of the resultant particles to the Tn-antigen was thereafter investigated.

3.1.1. Analysis of Tn-antigen expression level in SimpleCells (SC) by flow cytometry

To validate the specificity of the nanoparticles toward the Tn-antigen, MDA MB 231 SC and MCF7 SC breast as well as PC-3 SC prostate cancer cell lines were used, together with their WT counterparts as controls (Section 3, SI) [36,42]. As an extra control, non-cancerous HEK293T cells were used. The high level of Tn-antigen expression

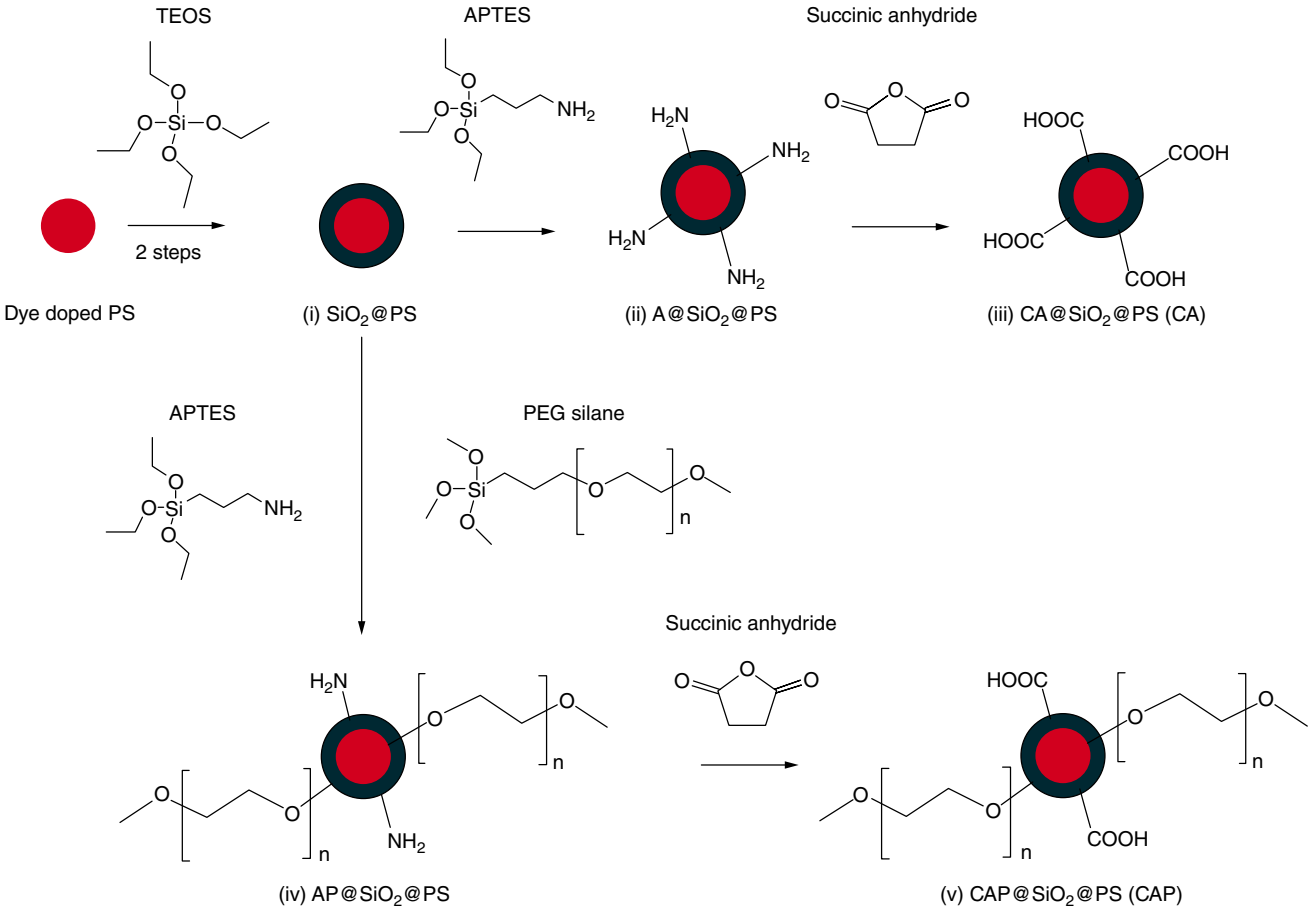

Figure 2. Synthesis scheme for **(i) SiO_2@PS**, **(ii) A@SiO_2@PS**, **(iii) CA@SiO_2@PS (CA)**, **(iv) AP@SiO_2@PS** and **(v) CAP@SiO_2@PS (CAP)**.

in the SC was confirmed via VVL staining using flow cytometry (Figure 4 and Supplementary Figure S6, SI section 8). The Median Fluorescence Intensity (MFI) is used here because the lectins are small enough to bind individual Tn-antigen units and therefore the total fluorescence emission observed from the bound lectins is proportional to the total amount of Tn-antigen present on the cell surface. The staining intensities of the MDA MB 231 SC, MCF7 SC and PC-3 SC cell lines were significantly higher than that of the corresponding non-engineered (WT) cells, indicating increased levels of Tn-antigen in SC. The relatively greatest difference in Tn-antigen expression was found in the MDA MB 231 SC, with 35-fold MFI compared with the WT. However, the MFIs for MCF7 SC and PC-3 SC were 6- and 10-fold higher compared with WT cells, respectively. The high expression of Tn-antigen in the SC makes these models suitable for the validation of the newly synthesized VVL-nanoparticle conjugates. A very low binding of VVL was found in the non-cancerous HEK293T cells. Density plots are presented in Supplementary Figure S6, SI section 8.

3.1.2. *Validation of VVL-labeled particle binding on Tn-antigen-expressing cancer cells by flow cytometry*

Initial tests showed that the nanoparticles **VVL-CA**, **VVL-CAP**, **CA** and **CAP** neither display toxicity to the cells nor affect their viability (Supplementary Figure S7, SI section 9). To validate particle binding on living cells, MDA MB 231 WT, MCF7 WT and PC-3 WT and the corresponding SCs together with non-cancerous HEK293T cells were incubated with **VVL-CA** and **VVL-CAP** as well as with their unlabeled (blank) control nanoparticles (**CA** and **CAP**) (Figure 5 & Supplementary Figure S8). Figure 5A shows density plots for MDA MB 231 cells incubated with **VVL-CA** and **VVL-CAP** (Section 10, SI for other cell lines). Figure 5B, C and D show the percentage of cells labeled with the different nanoparticles. The percentage of labeled cells was regarded as a more reliable measurement than MFI for evaluating the binding of particles. The particles have a significantly larger diameter (~80 nm) compared with lectins (up to several nm). This size difference prevents the particles from individually

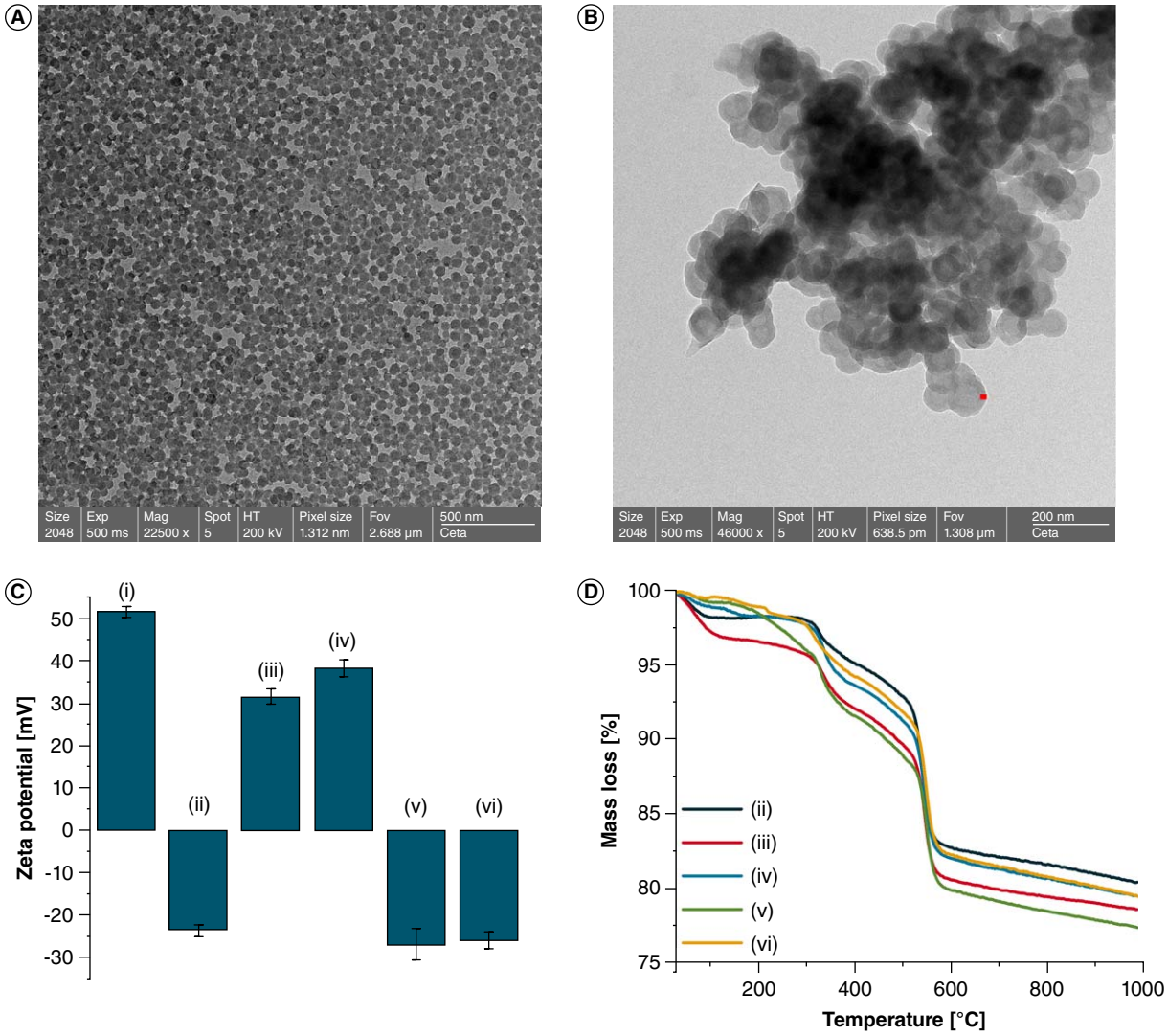

Figure 3. TEM images of **(A) PS** and **(B) SiO_2@PS**, with the red bar showing the silica shell thickness (ca. 18 nm). **(C)** Zeta potential measurements (in water, pH 6) and **(D)** TGA mass loss curves of **(i) PS**, **(ii) SiO_2@PS**, **(iii) A@SiO_2@PS**, **(iv) AP@SiO_2@PS**, **(v) CA** and **(vi) CAP**.o

binding to Tn-antigens on the cell surface. Additionally, in a physiological buffer, the particles can aggregate, leading to an artificial increase in the observed MFI. Therefore, we decided to use the percentage of labeled cells when studying the nanoparticles. When incubated with **VVL-CA** and **VVL-CAP**, 88.4% and 67.8% of the MDA MB 231 SC were labeled with the nanoparticles, respectively (Figure 5A). For MCF7 SC, the percentages were 67.2% (**VVL-CA**) and 17.9% (**VVL-CAP**). For PC-3 SC, the percentages for **VVL-CA** and **VVL-CAP** were 62.3% and 8.8% respectively (Supplementary Figure S8, SI). In all three SC cell lines, a significantly increased staining intensity was seen when incubated with **VVL-CA** compared with incubation with **CA**. This was also observed when compared with the corresponding WT cells (MDA MB 231: $p < 0.0001$; MCF7: $p = 0.0002$; PC-3: $p < 0.0001$; Figure 5B, C and D). For the MDA MB 231 cells, the engineered SCs also showed a significantly increased staining intensity compared with WT cells when incubated with **VVL-CAP** ($p < 0,0001$). However, no significantly increased staining intensity was observed between PC-3 and MCF7 SCs and WT cells when incubated with **VVL-CAP**.

Staining with **CA** and **CAP** particles was also observed for all cell lines, suggesting some unspecific binding (Figure 5 and SI section 10, Supplementary Figure S8). A very low binding was found on HEK293T cells for all particles which presumably represents the presence of some unspecific binding. Density plots for other cell lines (MCF7 WT, MCF7 SC, PC-3 WT, PC-3 SC and HEK293T) and particles are presented in Supplementary Figure S8, SI section 10.

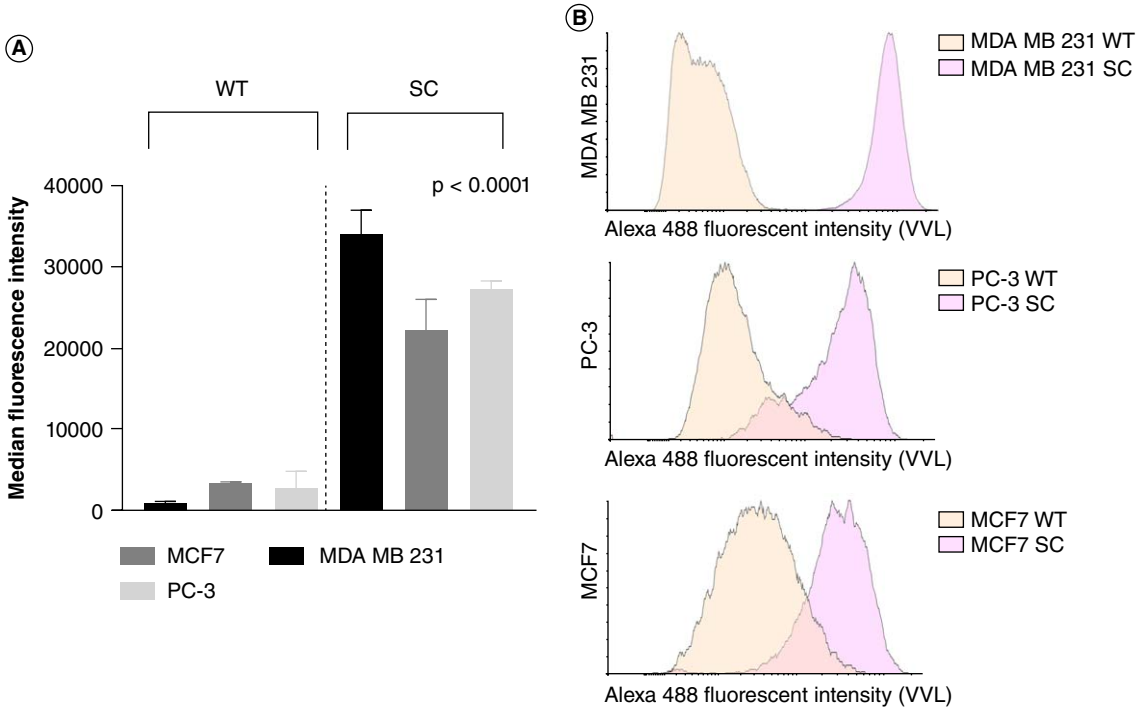

Figure 4. Flow cytometry analysis of Tn-antigen expression detected with VVL. MDA MB 231, MCF7 and PC3 WT and SC cells were stained with VVL (0.01 mg ml^{-1} in PBS). **(A)** Median fluorescent intensity graphs are shown. **(B)** Histograms show a shift in fluorescence intensity when incubating SC with VVL compared with WT incubated with VVL. The results (mean±SD of 2 parallel samples) for one experiment out of 3 with corresponding results are shown. P-values are shown as ****p $<$ 0.0001 (two-way ANOVA).

3.1.3. Confocal microscopy analysis of Tn-antigen-expressing cancer cell staining

The binding patterns of VVL, **VVL-CA** and **CA** were studied with a confocal microscope for all cell lines (Figures 6, 7 & Supplementary Figure S9, SI Section 11). For **VVL-CAP** and **CAP** binding we focused on MDA MB 231 cells because flow cytometry showed these results to be most promising. The VVL staining patterns of MDA MB 231, MCF7 and PC-3 show a clear increase of VVL in SC compared with WT. The staining of WT with VVL was mainly located in the intracellular parts of the cells, possibly representing the Golgi area and the endoplasmic reticulum (ER). In the SC, besides a strong intracellular staining, also a clear staining was seen on the plasma membrane (Figure 6).

The staining of the cells with **VVL-CA** (Figure 7A) nanoparticles displayed a localized staining pattern and a stronger staining in SC than in WT cells for the three cell lines. The positive staining observed with **VVL-CA** was located on the cell surface but did not show such a homogeneous coverage as observed with VVL. However, the binding pattern of **VVL-CAP** on MDA MB 231 was more continuous along the contour of the cells than on **VVL-CA**. Compared with VVL, intracellular staining was observed only to a minor extent in each cell type. The size of fluorescent particles (400 nm to 2 μm) varied suggesting the formation of particle aggregates. For **VVL-CA**, aggregates of different sizes can form in the buffer during the staining process, as is expected for particles suspended in a solution with high ionic strength [43]. The unlabeled control particles **CA** and **CAP** also displayed some non-specific binding to the cells (see Supplementary Figure S9, SI section 11).

In some cases, we saw binding of the **VVL-CA** and **VVL-CAP** outside the cellular area which was interpreted to be non-specific.

Z-stack confocal images of **VVL-CA** and **VVL-CAP**-labeled MDA MB 231 WT and SC (Supplementary Figure S10, SI section 11) show the distribution of the nanoparticles at different levels of the cells. It could be observed that more particles bound to MDA MB 231 SC than to WT. In addition, nanoparticles were detected in all layers and partly also on the coverslip. In agreement with the previous observation, **VVL-CA** seemed to form bigger aggregates than **VVL-CAP**.

3.1.4. Visualization of particles in SEM

Due to the varied size of the fluorescent particle formations observed in the confocal microscopy images, we postulated that aggregation of the particles occurred. According to Shrestha et al. [44] strong clustering of single nanoparticles is often observed when working

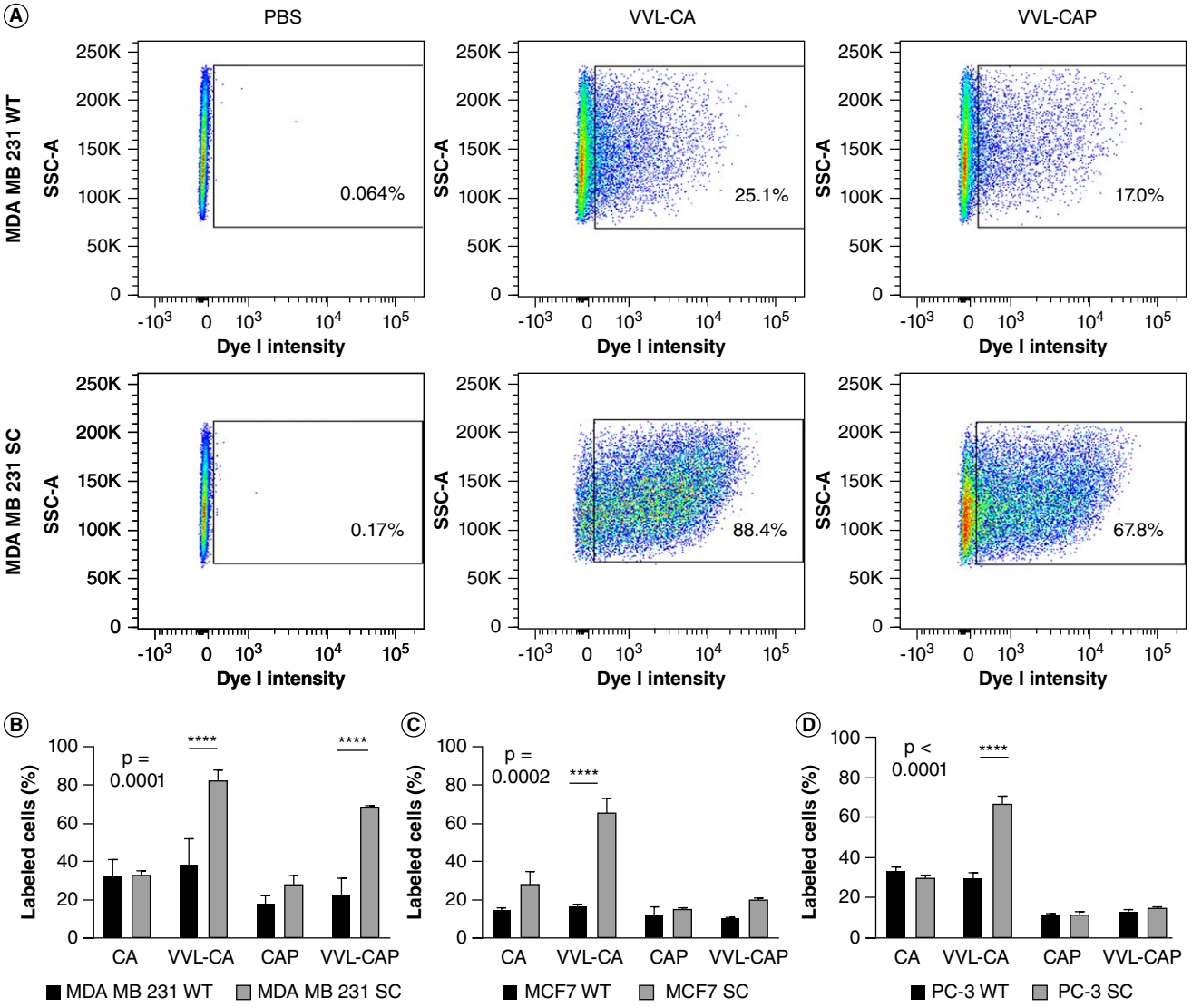

Figure 5. Nanoparticle staining of the different cell lines. **(A)** Density plots for MDA MB 231 WT (upper) and MDA MB 231 SC (lower) show the percentage of labeled cells in the absence (left) and the presence of nanoparticles **VVL-CA** (middle) and **VVL-CAP** (right). The percentage of cells labeled with the different nanoparticles are shown for **(B)** MDA MB 231, **(C)** MCF7 and **(D)** PC-3 cells. A difference in binding capacity between **VVL-CA** and **CA** was seen for the SCs (MDA MB 231: $p < 0.0001$; MCF7: $p = 0.0002$; PC-3: $p < 0.0001$). The overall interaction factor of the used two-way ANOVA gave a significance of $p = 0.0001$ (MDA MB 231); $p = 0.0002$ (MCF7) and $p < 0.0001$ (PC-3). Results show the mean±SD of 2 parallel samples in one experiment of three.

with nanoparticles. Compared with **VVL-CA**, **VVL-CAP** particles looked smaller and due to the lower fluorescent intensity, the smallest aggregates or single particles could have been undetectable. To investigate if this was the case in our study, Correlative Light and Electron Microscopy (CLEM) was utilized [45]. Correlative light and electron microscopy is a combination technique that helps avoid the shortcomings of these techniques when they are used separately [46]. It gives us the possibility to study our cells and particles in high resolution (EM) and at the same time gives us an overview of the different cells and localization of the fluorescent particles (confocal microscopy). Brightfield and fluorescence images were taken with a confocal microscope to localize cells and nanoparticles. Using gridded coverslips, the same cells (and nanoparticles) were detected and imaged with SEM. By this, we confirmed that the fluorescent signal seen in the confocal microscopy was coming from the nanoparticles. The overlay of the SEM and confocal images of the MDA MB 231 SC labeled with **VVL-CAP** showed that most of the nanoparticles were bound to the cells. The images also showed that discernible fluorescent particles formed differently-sized aggregates (Figure 8). In addition, an SEM picture at a lower magnification showed the presence of aggregates of different sizes on different parts of the cell (Figure 8).

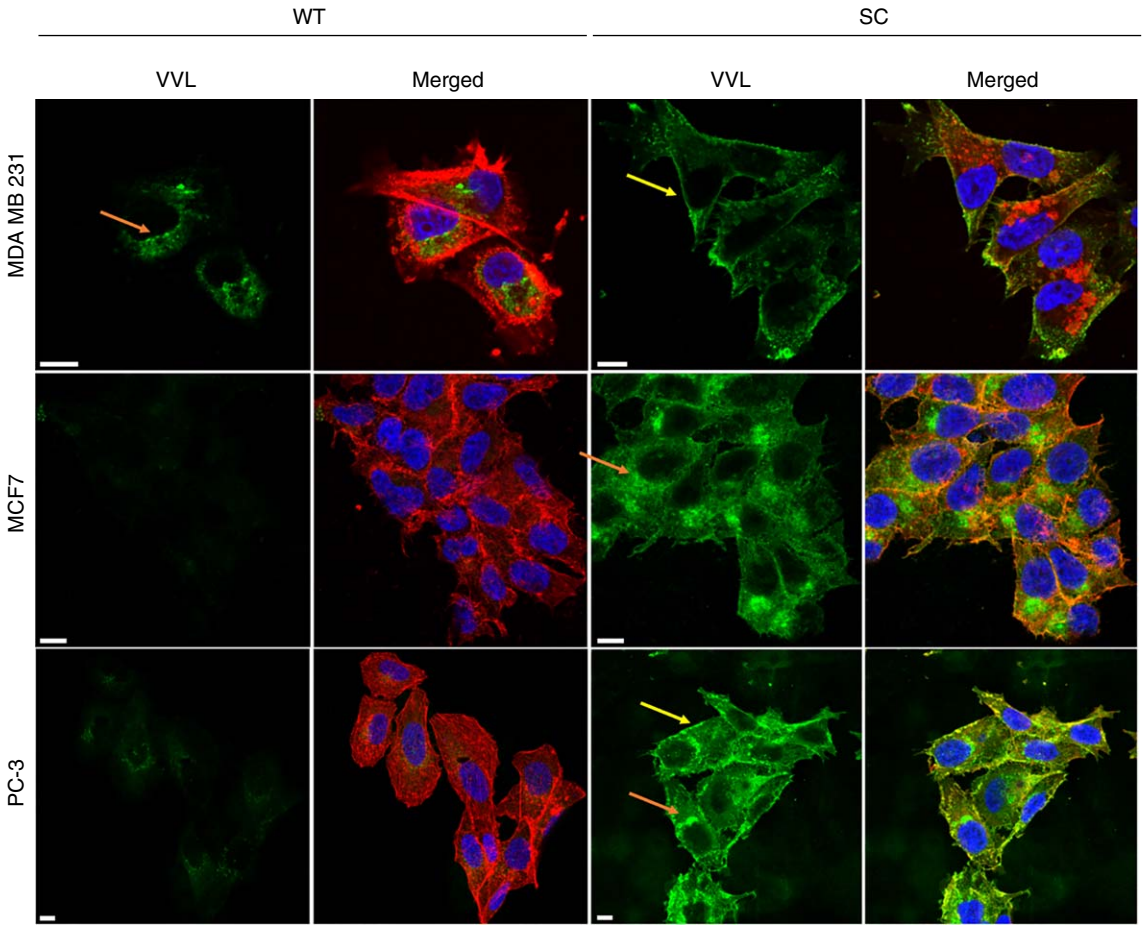

Figure 6. Visualization of the Tn-antigen with VVL. MDA MB 231, MCF7 and PC-3 WT (left) and SC (right) cells were stained with VVL. The yellow arrows show the plasma membrane staining (Tn-antigen present on the cell surface glycoproteins). The orange arrows show the intracellular staining. In addition, a merged picture is included for each cell line in which the Hoechst-stained nuclei (blue) and Phalloidin-stained F-actin (red) cytoplasmic structures are shown together with the VVL staining. One representative sample out of a minimum of two experiments is shown (Scale bar: 10 μm). The image adjustments were performed per cell line.

4. Discussion

The Tn-antigen is a shortened *O*-GalNAc glycan pattern that is frequently observed in several cancer types like breast, prostate, ovarian and colorectal cancer [13,15,47]. In these cells, the elongation of the *O*-GalNAc glycan is interrupted after the addition of the first GalNAc to the Ser or Thr in the newly synthesized protein [15]. Due to the frequent presence of the Tn-antigen in breast cancer (>80%) and prostate cancer (±4–26%), it has been studied as a promising tumor biomarker, particularly for early cancer forms [11–13]. Currently, Tn-antigen detection methods are mostly based on the use of lectins (e.g., HPA, VVL), antibodies (e.g., Remab6, 5F4, 1E3) and molecularly imprinted polymers [18,48–50].

In this study, we developed red dye-doped nanoparticles labeled with VVL and validated them for their ability to detect Tn-antigens in breast and prostate cancer cells. The particles have a PS core, which makes the synthesis and handling of nanometer-sized beads easier [39,40]. The core diameter of 40 ± 8 nm and a silica shell of 18 ± 2 nm result in a particle size of 76 ± 10 nm (Figure 3B). The red dye, emitting >650 nm (Figure 1B), reduces the background signal that occurs <650 nm due to cellular autofluorescence in the *in vitro* samples [51], and paves the way for possible future applications in the *in vivo* and *ex vivo* models. We used lectins as a glycan-recognizing tool. Even though they have been widely used, there are some disadvantages. One of the issues occurring in lectin use for the detection of glycans is the low binding affinity of the lectins toward the glycan. However, the binding affinity can be augmented by increasing the number of lectin-target interactions as in our case by binding a high number of lectins on one nanoparticle [23,32]. By this, the chances of binding to the glycan are increased. This will also have a positive effect on the selectivity of the lectins toward the glycan of interest [32,52]. On the other hand, fewer binding sites are needed to get a good fluorescence read-out

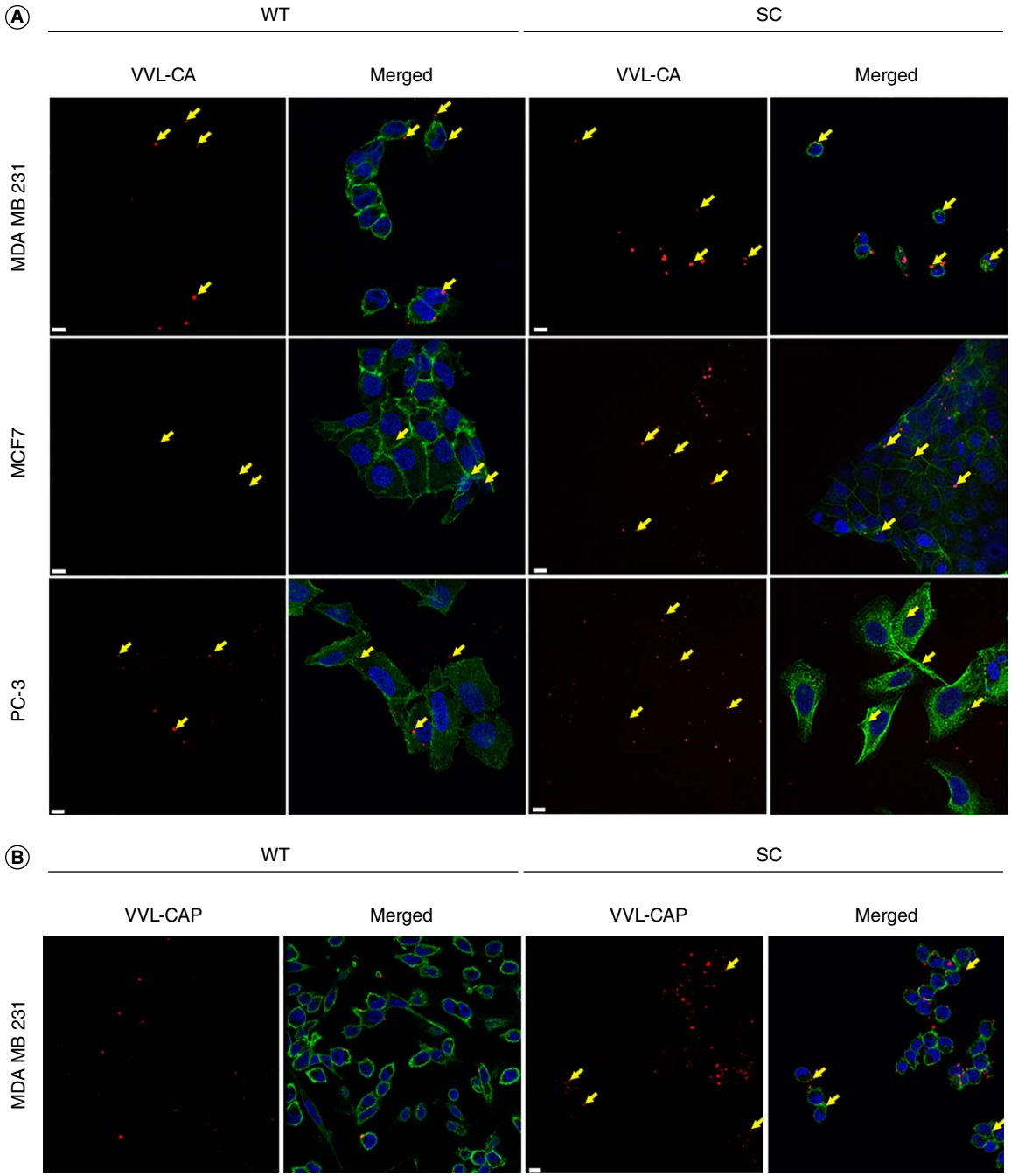

Figure 7. Visualization of the binding pattern of the nanoparticles to the cells. Staining of **(A)** MDA MB 231, PC3 and MCF7 WT and SC cells with **VVL-CA** and **(B)** MDA MB 231 with **VVL-CAP**. The merged figures show the particles (red), the nuclei (blue) and F-actin (green). Yellow arrows show nanoparticles bound to cells. One representative out of two experiments is shown. (Scale bar: 10 μm).

because the particles themselves are highly fluorescent. One would need more lectins to make binding visible with a microscope, for instance.

The MDA MB 231 and MCF7 breast cancer cell lines, and PC-3 prostate cancer cell line were used for the detection of truncated *O*-GalNAc glycans. Similar to many other established cancer cell lines [53], these cells express Tn-antigen at a much lower level than the tumor types they originate from [53,54]. To model the high Tn-antigen expression in breast tumors these WT breast cancer cell lines were glycoengineered via the SimpleCell technique to express corresponding high levels of Tn-antigen which was confirmed by flow cytometry of VVL-stained cells (Figure 4 & Supplementary Figure S5, SI). This staining demonstrates that SC cells are expressing Tn-antigen in high amounts, while WT cells show almost no staining.

The PEG groups were introduced on the surface of the particles to reduce non-specific binding events to non-

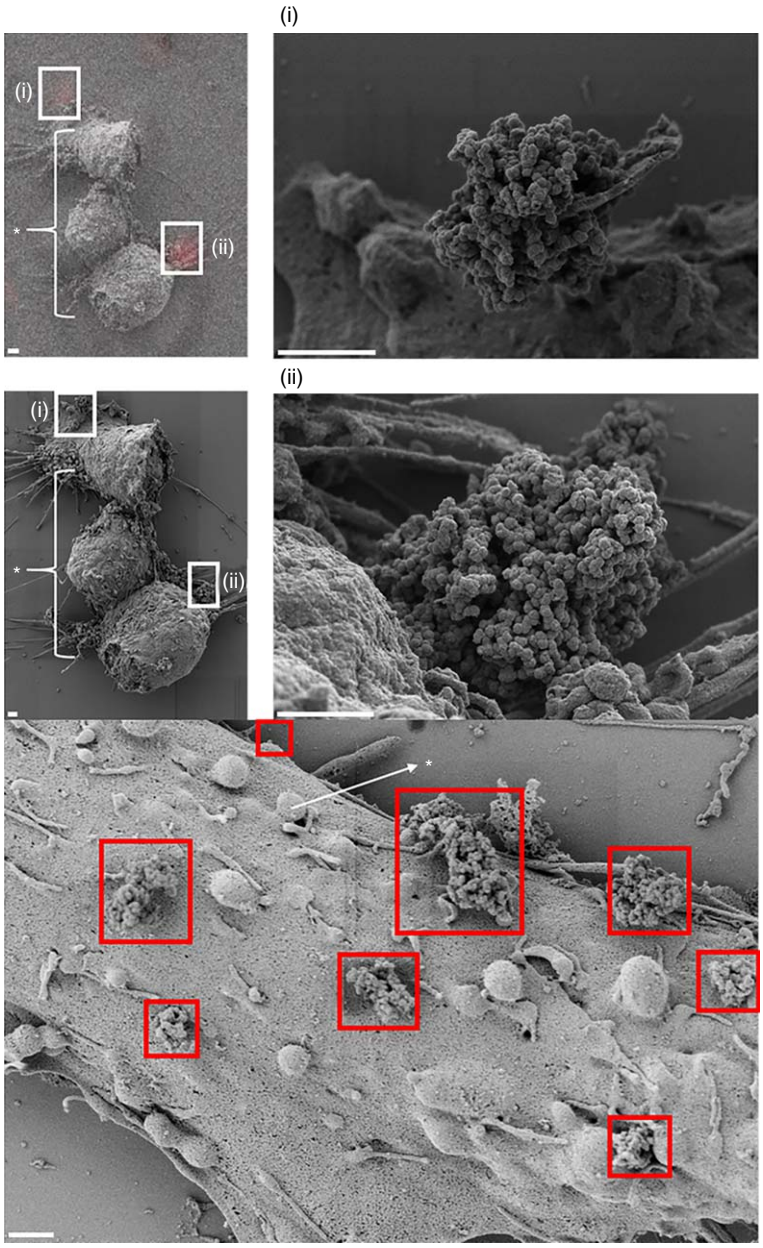

Figure 8. CLEM imaging of nanoparticle-labeled cells. Staining of MDA MB 231 SC with **VVL-CAP** imaged with confocal microscopy and SEM. Upper left panel: An overlay picture of SEM and a confocal microscopy image showing the location of the red fluorescent nanoparticles on the cells **(i, ii)**. Middle left panel: SEM picture of the same area. The white rectangular areas (i, ii) show the locations where the red fluorescence signal was detected. The star shows where the cells are located. A close-up image of the areas (i, ii) can be seen on the upper right panel **(i)** and middle right panel **(ii)** (magnification: 25 400 x). The lower panel shows a cell at a lower magnification (8467 x). The red squares show nanoparticle aggregates of different sizes.

target molecules [27]. The binding of both **VVL-CA** and **VVL-CAP** to MDA MB 231 SC was increased compared with the unlabeled particles and WT cells but PEGylation did not seem to have much effect on the staining of MDA MB 231 SC or WT cells although the particles seemed to form smaller fluorescent spots in **VVL-CAP**- than in **VVL-CA**-stained cells. PEG is more hydrophilic and thus more soluble in aqueous media, which may explain the presence of smaller clusters in **VVL-CAP** than in **VVL-CA**-stained cells (Figure 7A for **VVL-CA** and Figure 7B for **VVL-CAP**). Under *in vivo* conditions, PEGylation is known to markedly increase the accessibility of the particles to the target organs and cells by opposing their removal from the circulation and the extracellular fluids by the phagocytosing cells [55]. It is involved in decreasing the protein corona effect, which means the unspecific protein binding to the nanoparticles [56]. However, under *in vitro* conditions, using different cell models and particles,

PEGylation has been found to decrease the binding of the particles to the target proteins on the cell surface [57]. PEGylation may have a corresponding effect in our *in vitro* setting. However, particles lacking VVL (**CA** and **CAP**) serving as blank particles, indicated some non-specific binding. Staining with **CA** and **CAP** demonstrates that non-specific binding is not influenced by cell type (SC or WT), indicating that binding occurs independently of Tn-antigen expression. The results with MCF7 and PC-3 were comparable to those of MDA MB 231 except that **VVL-CAP** particles were not specifically bound to SC. The cell surface composition of proteins on the surface of these cells may hinder the PEGylated VVL-particles from binding the Tn-antigen motifs on the cell surface proteins [58].

Different VVL or particle staining of the used cancer cell lines may be caused by levels of *O*-GalNAc glycosylation which depends on the cell-specific expression of one or several of the 20 ppGalNAc-Ts and the cell-specific array of the glycoproteins on the cell surface. Other factors contributing to the level of glycosylation are cell-specific signaling, oxygen level, temperature, pH and in tumors, the microenvironment [54,59,60]. Staining of MDA MB 231 SC with VVL was more effective compared with that of MCF7 SC and PC-3 SC (Figure 4), suggesting higher expression of Tn-antigen in these cells. This was also evident following staining with **VVL-CA** showing that the labeling with the particles is in line with the results from VVL staining. However, a higher staining efficiency of SC was observed for **VVL-CA** than for **VVL-CAP**. This difference was bigger in MCF 7 and PC-3 cells compared with MDA MB 231.

In the confocal microscopic images, we observed VVL staining of the cell surface as well as on intracellular structures like the Golgi area and ER. VVL can most probably be endocytosed and bind Tn-antigen-expressing structures inside the cells. The capacity of internalization can differ between the cell lines. The initiation of *O*-glycosylation and transfer of a GalNAc on the Ser or Thr normally occurs in the Golgi [61,62] but particularly in cancer cells, GalNAc transferases can relocalize to ER with marked functional consequences [63,64]. Intracellular staining of the cells with the VVL-labeled nanoparticles was only observed in a small amount. This was probably attributed to the larger dimensions of the particles, their structural rigidity and possible particle aggregation in contrast to the lectins.

To investigate if particles were aggregated and if single particles could be observed, we used Correlative Light and Electron Microscopy (CLEM) [45]. CLEM has previously been applied to check cell binding of the particles by Vancová and coworkers, who used gold nanoparticles and quantum dots for the detection of core fucosylated glycans [65]. The results showed that the particles were present in differently-sized aggregates. No single particles attached to the cells were detected which could be either due to the resolution limits of the microscope or due to the removal of the particles during the washing process of sample preparation for scanning electron microscopy. The fixation procedure could also induce particle aggregation though, based on TEM imaging, the particles themselves may be prone to form clusters.

5. Conclusion

The experimental results suggest that the VVL-labeled nanoparticles could be applied to detecting Tn-antigen-expressing cancer cells in the clinical setting. They could be suitable for the demonstration of Tn-antigen-expressing living cancer cells such as circulating tumor cells in patient blood samples and in the follow-up of tumor progression, and treatment responses [66]. The particles could also be used *ex vivo* for the demonstration of Tn-antigen-expressing cancer cells by staining cell smears or cryosections of tumor samples. However, optimization of the particles and the PEGylation process would be needed to decrease the aggregation and non-specific staining and increase the specific binding of the particles. Particularly, a higher fluorescence intensity of the particles would help the microscopic analysis and quantification of Tn-antigen-expressing cancer cells. In addition, the use of these particles makes it possible to label them with different lectins at the same time. This would increase the possibility of detecting a specific cancer-cell type. The advantage of these particles is that the dye can be changed which gives a variety of possible combinations of dyes with increased intensity and lectin-labeled particles for future studies. In the future, this type of nanoparticles could be further developed to be applied in targeting Tn-antigen-expressing cancer cells for specific therapies *in vivo* [67]. The combination of lectins and red-dye doped nanoparticles, applying the concept presented here could also be explored for the detection of other cancer-specific changes with these nanoparticles conjugated with an appropriate lectin or glycan-binding antibody. The use of engineered lectins could further optimize the use of our particles [52].

Article highlights

- New VVL-labeled fluorescent red dye-doped silica-coated PS particles were developed and tested for detection of Tn-antigen, expressed only in malignant cells.
- Breast and prostate cancer cell lines gene-engineered to express Tn-antigen at a high level and non-engineered counterparts were used as models.
- The VVL-labeled particles bound specifically and effectively to Tn-antigen-expressing cells compared with their control cells as shown by flow cytometry.

- Confocal microscopy showed that the VVL-labeled particles were bound to the cell surface of target cells, mostly as aggregates.
- Further optimization to increase the intensity of the fluorescence and decrease the aggregation tendency of particles would help detect single particles.
- The VVL-labeled nanoparticles could be used for recognizing Tn-antigen-expressing cells (circulatory tumor cells) in blood samples of breast and prostate cancer patients, biopsies, or cryosections of tumor samples. In the future, they could also be developed to function *in vivo* as carriers for targeted therapy of Tn-antigen-expressing cancer.

Author contributions

A Verhassel: methodology, investigation, data analysis, visualization, writing - original draft, writing – review & editing. M Kimani: methodology, investigation, data analysis, visualization, writing - original draft, writing – review & editing. K Gidwani: methodology, writing – review & editing. J Sandholm: methodology, supervision, visualization, writing – review & editing, K Gawliza: conceptualization, methodology, supervision, visualization, writing – review & editing. K Rurack: conceptualization, funding acquisition, resources, writing – review & editing. P Härkönen: conceptualization, funding acquisition, resources, supervision, writing – review & editing.

Financial disclosure

The study was funded as part of the European Network 'GlycoImaging' by the European Union's Horizon 2020 research and innovation program under the Marie Skłodowska-Curie Action grant agreement No. 721297.

Working grants were received from the University of Turku Graduate School (Drug Research Doctoral Programme), Ida Montinin Säätiö (The Ida Montin Foundation), K. Albin Johansson Foundation, Paulo Foundation and Lounais-Suomen Syöpäyhdistys (The Cancer Society of Southwestern Finland).

The authors have no other relevant affiliations or financial involvement with any organization or entity with a financial interest in or financial conflict with the subject matter or materials discussed in the manuscript apart from those disclosed.

Competing interests disclosure

The authors have no competing interests or relevant affiliations with any organization or entity with the subject matter or materials discussed in the manuscript. This includes employment, consultancies, honoraria, stock ownership or options, expert testimony, grants or patents received or pending, or royalties.

Writing disclosure

No writing assistance was utilized in the production of this manuscript.

ORCID

Alejandra Verhassel https://orcid.org/0009-0006-7289-2791
Martha Kimani https://orcid.org/0000-0002-1292-9795
Kamlesh Gidwani https://orcid.org/0000-0002-9014-0618
Jouko Sandholm https://orcid.org/0000-0003-0638-2444
Kornelia Gawlitza https://orcid.org/0000-0002-2043-4522
Knut Rurack https://orcid.org/0000-0002-5589-5548
Pirkko Härkönen https://orcid.org/0000-0001-9440-9971

References

Papers of special note have been highlighted as: • of interest; •• of considerable interest

1. Reily C, Stewart TJ, Renfrow MB, et al. Glycosylation in health and disease. Nat Rev Nephrol. 2019;15(6):346–366. doi:10.1038/s41581-019-0129-4
   • This paper gives a clear overview of glycobiology and focuses on its role in diseases such as cancer.
2. Varki A. Biological roles of glycans. Glycobiology. 2017;27(1):3–49. doi:10.1093/glycob/cww086
3. Schjoldager KT, Narimatsu Y, Joshi HJ, et al. Global view of human protein glycosylation pathways and functions. Nat Rev Mol Cell Biol. 2020;21(12):729–749. doi:10.1038/s41580-020-00294-x
   • Here a clear overview of the different types of glycosylation is explained
4. Fu C, Zhao H, Wang Y, et al. Tumor-associated antigens: tn-antigen, sTn-antigen, and T antigen. HLA. 2016;88(6):275–286. doi:10.1111/tan.12900
   • This paper gives an overview of aberrant O-glycans and their role in cancer.
5. Dube DH, Bertozzi CR. Glycans in cancer and inflammation–potential for therapeutics and diagnostics. Nat Rev Drug Discov. 2005;4:477–488. doi:10.1038/nrd1751
6. Adamczyk B, Tharmalingam T, Rudd PM. Glycans as cancer biomarkers. Biochim Biophys Acta. 2012;1820(9):1347–1353. doi:10.1016/j.bbagen.2011.12.001
7. Thomas D, Rathinavel AK, Radhakrishnan P. Altered glycosylation in cancer: a promising target for biomarkers and therapeutics. Biochim Biophys Acta- Rev Cancer. 2021;1875(1):188464. doi:10.1016/j.bbcan.2020.188464
8. Costa AF, Campos D, Reis CA, et al. Targeting Glycosylation: A New Road for Cancer Drug Discovery. Trends Cancer. 2020;6(9):757–766. doi:10.1016/j.trecan.2020.04.002
9. Brockhausen I. Pathways of O-glycan biosynthesis in cancer cells. Biochim Biophys Acta-Gen Subj. 1999;1473(1):67–95. doi:10.1016/S0304-4165(99)00170-1
10. Itzkowitz SH, Yuan M, Montgomery CK, et al. Expression of Tn, Sialosyl-Tn, and T Antigens in Human Colon Cancer. Cancer Res. 1989;49(1):197 LP–204.
11. Konska G, Guerry M, Caldefie-Chezet F, et al. Study of the expression of Tn-antigen in different types of human breast cancer cells using VVA-B4 lectin. Oncol Rep. 2006;15(2):305–310. doi:10.3892/OR.15.2.305
12. Kumar SR, Sauter ER, Quinn TP, et al. Thomsen-Friedenreich and Tn-antigens in Nipple Fluid: Carbohydrate Biomarkers for Breast Cancer Detection. Clin Cancer Res. 2005;11(19):6868–6871. doi:10.1158/1078-0432.CCR-05-0146
13. Li Q, Anver MR, Butcher DO, et al. Resolving conflicting data on expression of the Tn-antigen and implications for clinical trials with cancer vaccines. Mol Cancer Ther. 2009;8(4):971–979. doi:10.1158/1535-7163.MCT-08-0934
14. Babino A, Oppezzo P, Bianco S, et al. Tn-antigen is a pre-cancerous biomarker in breast tissue and serum in

n-nitrosomethylurea-induced rat mammary carcinogenesis. Int J Cancer. 2000;86(6):753–759. doi:10.1002/(sici)1097-0215(20000615)86:6⟨753::aid-ijc1⟩3.0.co;2-#
15. Ju T, Aryal RP, Kudelka MR, et al. The Cosmc connection to the Tn-antigen in cancer. Cancer Biomark. 2014;14(1):63–81. doi:10.3233/CBM-130375
16. Szczykutowicz J, Tkaczuk-Włach J, Ferens-Sieczkowska M. Glycoproteins Presenting Galactose and N-Acetylgalactosamine in Human Seminal Plasma as Potential Players Involved in Immune Modulation in the Fertilization Process. Int J Mol Sci. 2021;22(14):7331. doi:10.3390/ijms22147331
17. Poiroux G, Barre A, van Damme EJM, et al. Plant Lectins Targeting O-Glycans at the Cell Surface as Tools for Cancer Diagnosis, Prognosis and Therapy. Int J Mol Sci. 2017;18(6):1232. doi:10.3390/ijms18061232
18. Matsumoto Y, Kudelka MR, Hanes MS, et al. Identification of Tn-antigen O-GalNAc-expressing glycoproteins in human carcinomas using novel anti-Tn recombinant antibodies. Glycobiology. 2020;30(5):282–300. doi:10.1093/glycob/cwz095
19. S Silva ML, Rangel MGH. A Vicia villosa agglutinin biosensor for cancer-associated Tn-antigen. Sens Actuators B Chem. 2017;252:777–784. doi:10.1016/j.snb.2017.06.021
20. Pinto R, Carvalho AS, Conze T, et al. Identification of new cancer biomarkers based on aberrant mucin glycoforms by *in situ* proximity ligation. J Cell Mol Med. 2012;16(7):1474–1484. doi:10.1111/j.1582-4934.2011.01436.x
21. Liyanage SH, Yan M. Quantification of binding affinity of glyconanomaterials with lectins. Chem Commun (Camb). 2020;56(88):13491–13505. doi:10.1039/d0cc05899h]
22. Loureiro LR, Carrascal MA, Barbas A, et al. Challenges in antibody development against Tn and Sialyl-Tn-antigens. Biomolecules. 2015;5:1783–1809.
23. Gidwani K, Huhtinen K, Kekki H, et al. A nanoparticle-lectin immunoassay improves discrimination of serum CA125 from malignant and benign sources. Clin. Chem. 2016;62(10):1390–1400. doi:10.1373/clinchem.2016.257691
•• In this paper, the researchers focus on serum cancer antigen 125 (CA125) and explain in detail the benefit of using lectin-labeled particles over lectins only.
24. Gidwani K, Nadeem N, Huhtinen K, et al. Europium Nanoparticle-Based Sialyl-Tn Monoclonal Antibody Discriminates Epithelial Ovarian Cancer-Associated CA125 from Benign Sources. J Appl Lab Med. 2019;4(3):299–310. doi:10.1373/jalm.2018.028266
25. Curtis EM, Bahrami AH, Weikl TR, et al. Modeling nanoparticle wrapping or translocation in bilayer membranes. Nanoscale. 2015;7(34):14505–14514. doi:10.1039/c5nr02255j
26. Rees P, Wills JW, Brown MR, et al. The origin of heterogeneous nanoparticle uptake by cells. Nat Commun. 2019;10:2341. doi:10.1038/s41467-019-10112-4
27. Sarma D, Carl P, Climent E, et al. Multifunctional Polystyrene Core/Silica Shell Microparticles with Antifouling Properties for Bead-Based Multiplexed and Quantitative Analysis. ACS Appl Mater Interfaces. 2019;11(1):1321–1334. doi:10.1021/acsami.8b10306
28. Tobias C, Climent E, Gawlitza K, et al. Polystyrene Microparticles with Convergently Grown Mesoporous Silica Shells as a Promising Tool for Multiplexed Bioanalytical Assays. ACS Appl Mater Interfaces. 2021;13(1):207–218. doi:10.1021/acsami.0c17940
29. Behnke T, Würth C, Hoffmann K, et al. Encapsulation of Hydrophobic Dyes in Polystyrene Micro- and Nanoparticles via Swelling Procedures. J Fluoresc. 2011;21(3):937–944. doi:10.1007/s10895-010-0632-2
30. Behnke T, Mathejczyk JE, Brehm R, et al. Target-specific nanoparticles containing a broadband emissive NIR dye for the sensitive detection and characterization of tumor development. Biomaterials. 2013;34(1):160–170. doi:10.1016/j.biomaterials.2012.09.028
31. Zhu H, McShane MJ. Loading of Hydrophobic Materials into Polymer Particles: Implications for Fluorescent Nanosensors and Drug Delivery. J. Am. Chem. Soc. 2005;127(39):13448–13449. doi:10.1021/ja052188y
32. Haab BB. Using lectins in biomarker research: addressing the limitations of sensitivity and availability. PROTEOMICS - Clinical Applications. 2012;6(7-8):346–350. doi:10.1002/PRCA.201200014
33. Yang X, Sun Y, Xiang Y, et al. Controlled synthesis of PEGylated surface protein-imprinted nanoparticles. Analyst. 2019;144(18):5439–5448. doi:10.1039/c9an01221d
34. Han X, Han W, Zhang S, et al. PEGylation of protein-imprinted nanocomposites sandwiching CdTe quantum dots with enhanced fluorescence sensing selectivity. RSC Adv. 2019;9(65):38165–38173. doi:10.1039/c9ra08556d
35. Chen B, Zuberi M, Ben Borgens R, et al. Affinity for, and Localization of, PEG-Functionalized Silica Nanoparticles to Sites of Damage in an *Ex Vivo* Spinal Cord Injury Model. J Biol Eng. 2012;6(1):18. doi:10.1186/1754-1611-6-1827
36. Steentoft C, Vakhrushev SY, Joshi HJ, et al. Precision mapping of the human O-GalNAc glycoproteome through SimpleCell technology. EMBO J. 2013;32(10):1478–1488. doi:10.1038/emboj.2013.79
•• In this paper researchers explain the strategy of the SimpleCell Technique and O-glycoproteome in more detail and focus on different human cell lines; including the cell lines used in this paper.
37. Ju T, Cummings RD. A unique molecular chaperone Cosmc required for activity of the mammalian core 1 beta 3-galactosyltransferase. Proc Natl Acad Sci USA. 2002;99(26):16613–16618. doi:10.1073/pnas.262438199
38. Xu J, Zhu L, Wang Q, et al. meso-C6F5 substituted BODIPYs with distinctive spectroscopic properties and their application for bioimaging in living cells. Tetrahedron. 2014;70(35):5800–5805. doi:10.1016/j.tet.2014.06.040
39. Ernawati L, Balgis R, Ogi T, et al. Role of Acetone in the Formation of Highly Dispersed Cationic Polystyrene Nanoparticles. Chem Process Eng. 2017;38(1):5800–5805. doi:10.1515/cpe-2017-0002
40. Nandiyanto ABD, Suhendi A, Ogi T, et al. Synthesis of additive-free cationic polystyrene particles with controllable size for hollow template applications. Colloids Surf A Physicochem Eng Asp. 2012;396:96–105. doi:10.1016/j.colsurfa.2011.12.048
41. Stöber W, Fink A, Bohn E. Controlled growth of monodisperse silica spheres in the micron size range. Journal of Colloid and Interface Science. 1968;26(1):62–69. doi:10.1016/0021-9797(68)90272-5

42. Steentoft C, Vakhrushev SY, Vester-Christensen MB, et al. Mining the O-glycoproteome using zinc-finger nuclease-glycoengineered SimpleCell lines. Nat Methods. 2011;8(11):977–982. doi:10.1038/nmeth.1731
•• This paper discusses the SimpleCell technology and its benefits.
43. Wang L, Yang X, Wang Q, et al. Effects of ionic strength and temperature on the aggregation and deposition of multi-walled carbon nanotubes. J Environ Sci. 2017;51:248–255. doi:10.1016/j.jes.2016.07.003
44. Shrestha S, Wang B, Dutta P. Nanoparticle processing: understanding and controlling aggregation. Adv. Colloid Interface Sci. 2020;279:102162. doi:10.1016/J.CIS.2020.102162
45. Rilla K, Koistinen A. Correlative light and electron microscopy reveals the HAS3-induced dorsal plasma membrane ruffles. Int J Cell Biol. 2015;2015:769163. doi:10.1155/2015/769163
46. De Boer P, Hoogenboom JP, Giepmans BNG. Correlated light and electron microscopy: ultrastructure lights up! Nature Methods. 2015;12(6):503–513. doi:10.1038/nmeth.3400
47. Ogawa H, Ghazizadeh M, Araki T. Tn and sialyl-Tn-antigens as potential prognostic markers in human ovarian carcinoma. Gynecol Obstet Invest. 1996;41(4):278–283. doi:10.1159/000292284
48. Bojar D, Meche L, Meng G, et al. A Useful Guide to Lectin Binding: Machine-Learning Directed Annotation of 57 Unique Lectin Specificities. ACS Chem Biol. 2022;17(11):2993–3012. doi:10.1021/acschembio.1c00689
49. Thurnher M, Clausen H, Sharon N, et al. Use of O-Glycosylation-Defective Human Lymphoid Cell Lines and Flow Cytometry to Delineate the Specificity of Moluccella Laevis Lectin and Monoclonal Antibody 5F4 for the Tn-antigen (GalNAcel-O-Ser/Thr). Immunol. Lett. 1993;36(3):239–243. doi:10.1016/0165-2478(93)90095-j
50. Palladino P, Papi F, Minunni M, et al. Structurally Constrained MUC1-Tn Mimetic Antigen as Template for Molecularly Imprinted Polymers (MIPs): A Promising Tool for Cancer Diagnostics. Chempluschem. 2022;87(9):e202200068. doi:10.1002/cplu.202200068
51. Staudinger C, Borisov SM. Long-wavelength analyte-sensitive luminescent probes and optical (bio)sensors. Methods Appl Fluoresc. 2015;3(4):042005. doi:10.1088/2050-6120/3/4/042005
52. Tommasone S, Allabush F, Tagger YK, et al. The challenges of glycan recognition with natural and artificial receptors. Chem Soc Rev. 2019;48(22):5488–5505. doi:10.1039/C8CS00768C
53. Sun X, Ju T, Cummings RD. Differential expression of Cosmc, T-synthase and mucins in Tn-positive colorectal cancers. BMC Cancer. 2018;18(1):827. doi:10.1186/s12885-018-4708-8
54. Radhakrishnan P, Dabelsteen S, Madsen FB, et al. Immature truncated O-glycophenotype of cancer directly induces oncogenic features. Proc Natl Acad Sci USA. 2014;111(39):E4066–E4075. doi:10.1073/pnas.1406619111
55. Seib FP, Patel AK, El-Baz N, et al. The impact of PEGylation on cellular uptake and *in vivo* biodistribution of gold nanoparticle MRI contrast agents. Bioengineering. 2022;9(12):766. doi:10.3390/bioengineering9120766
56. Forgham H, Zhu J, Zhang T, et al. Fluorine-modified polymers reduce the adsorption of immune-reactive proteins to PEGylated gold nanoparticles. Nanomedicine (London, England). 2024;19(11):995–1012. doi:10.2217/nnm-2023-0357
57. Hama S, Itakura S, Nakai M, et al. Overcoming the polyethylene glycol dilemma via pathological environment-sensitive change of the surface property of nanoparticles for cellular entry. J Control Release. 2015;206:67–74. doi:10.1016/j.jconrel.2015.03.011
58. Fang Y, Xue J, Gao S, et al. Cleavable PEGylation: a strategy for overcoming the "PEG dilemma" in efficient drug delivery. Drug Delivery. 2017;24(2):22. doi:10.1080/10717544.2017.1388451
59. Peixoto A, Fernandes E, Gaiteiro C, et al. Hypoxia enhances the malignant nature of bladder cancer cells and concomitantly antagonizes protein O-glycosylation extension. Oncotarget. 2016;7(39):63138–63157. doi:10.18632/oncotarget.11257
60. Kim SM, Chang KH, Oh DJ. Effect of environmental parameters on glycosylation of recombinant immunoglobulin G produced from recombinant CHO cells. Biotechnol Bioprocess Eng. 2018;23(4):456–464. doi:10.1007/s12257-018-0109-8
61. Park JH, Nishidate T, Kijima K, et al. Critical roles of mucin 1 glycosylation by transactivated polypeptide N-acetylgalactosaminyltransferase 6 in mammary carcinogenesis. Cancer Res. 2010;70(7):2759–2769. doi:10.1158/0008-5472.CAN-09-3911
62. Gupta R, Leon F, Rauth S, et al. A systematic review on the implications of O-linked glycan branching and truncating enzymes on cancer progression and metastasis. Cells. 2020;9(2):446. doi:10.3390/cells9020446
63. Gill DJ, Tham KM, Chia J, et al. Initiation of GalNAc-type O-glycosylation in the endoplasmic reticulum promotes cancer cell invasiveness. Proc Natl Acad Sci USA. 2013;110(34):E3152–E3161. doi:10.1073/pnas.1305269110
64. Nguyen AT, Chia J, Ros M, et al. Organelle specific O-glycosylation drives MMP14 activation, tumor growth, and metastasis. Cancer Cell. 2017;32(5):639–653.e6. doi:10.1016/J.CCELL.2017.10.001
65. Vancová M, Nebesářová J. Correlative fluorescence and scanning electron microscopy of labeled core fucosylated glycans using cryosections mounted on carbon-patterned glass slides. PLOS ONE. 2015;10(12):e0145034. doi:10.1371/JOURNAL.PONE.0145034
66. Huang Q, Wang Y, Chen X, et al. Nanotechnology-based strategies for early cancer diagnosis using circulating tumor cells as a liquid biopsy. Nanotheranostics. 2018;2(1):21–41. doi:10.7150/ntno.22091
67. Mitchell MJ, Billingsley MM, Haley RM, et al. Engineering precision nanoparticles for drug delivery. Nat Rev Drug Discov. 2021;20(2):101–124. doi:10.1038/s41573-020-0090-8